

**First-principles study of Zintl aluminide SrAl<sub>2</sub>**

Alexander Slepko and Alexander A. Demkov\*

*Department of Physics, The University of Texas at Austin, Austin, Texas 78712, USA*

(Received 3 February 2012; published 29 May 2012)

Zintl intermetallics hold promise for applications in oxide/semiconductor epitaxy. We report a density functional investigation of the Zintl phase strontium aluminide SrAl<sub>2</sub>. We calculate electronic properties of the orthorhombic and cubic phases. For the orthorhombic phase, we calculate the work function and surface energy for (001), (010), and (100) orientated surfaces. The work function varies between 2.0 eV and 4.1 eV, and it is determined by the predominant atomic species on the surface. The surface energy ranges from 320 erg/cm<sup>2</sup> to 1842 erg/cm<sup>2</sup>. We also calculate the elastic constants.

DOI: [10.1103/PhysRevB.85.195462](https://doi.org/10.1103/PhysRevB.85.195462)

PACS number(s): 73.30.+y, 73.40.Ns

**I. INTRODUCTION**

Silicon-based complementary metal oxide semiconductor (CMOS) technology is rapidly approaching its physical limits.<sup>1,2</sup> The most recent problem has been the thickness of the SiO<sub>2</sub> gate oxide, which current technology has not been able to reduce below the critical thickness of four atomic layers without losing its insulating properties. The current solution to the problem is to use a gate oxide with a dielectric constant higher than that of SiO<sub>2</sub>, such as hafnia, allowing for higher gate capacitance, albeit operating well above the physical size limit.<sup>3</sup> Using crystalline perovskites as a gate dielectric may offer further gate stack scaling.<sup>4</sup> For comparison, the relative dielectric constant of SiO<sub>2</sub> is approximately 4, while that of SrTiO<sub>3</sub> is 2000.<sup>5</sup> However, despite the promise, incorporating crystalline oxides on silicon imposes several difficulties.<sup>6,7</sup> One arises from the abrupt change in the nature of chemical bonding across the Si/dielectric interface. While Si forms a covalent bond network, bonding in a perovskite such as SrTiO<sub>3</sub>, for example, is largely ionic. Thus, an epitaxial oxide/semiconductor interface is likely to suffer from high interfacial energy caused by the transition from the ionic to covalent bond type. This in turn prevents the oxide from wetting the Si substrate necessary for a layer-by-layer growth of high-quality films. In the case of SrTiO<sub>3</sub> (STO) on Si, the surface energy of STO plus the energy of the interface should not exceed the surface energy of Si of ~1700 erg/cm<sup>2</sup> to achieve wetting. With the STO surface energy ranging from 800 to 2000 erg/cm<sup>2</sup>, depending on the environment, one needs an interface with an energy below 900 erg/cm<sup>2</sup> to wet silicon.<sup>7</sup> One possible solution to this problem is incorporating a mediating interfacial layer that can accommodate both the oxide's ionic bonding and semiconductor's covalent bonding. For STO on Si, this has been realized with the SrSi<sub>2</sub> template, which has the stoichiometry of a bulk Zintl-Klemm intermetallic compound.<sup>8,9</sup> These unusual materials were first characterized by Eduard Zintl in the 1930s.<sup>10</sup> Typically, Zintl phases are of the form A<sub>a</sub>X<sub>x</sub> = (A<sup>n+</sup>)<sub>a</sub>[X<sup>(an/x)-</sup>]<sub>x</sub>, where the atomic species A, called the "active" metal, is of the first or second main group in the periodic table, and species X is an electronegative metal or a semimetal of the third or fourth main group. The active metal donates its valence electrons to the electronegative metal, and both species can build seemingly independent sublattices in the so-called Zintl phase. The sublattice of species X typically assumes the coordinated

structure capable of accommodating extra electrons in its bonds (Zintl-Klemm rules<sup>11</sup>), and thus effectively shows the covalent bonding character of the isovalent element. For example, in the prototypical Zintl phase NaTl, the Tl sublattice assumes the diamond structure of the neighboring elements Si or C upon receiving the extra electron from Na.<sup>11</sup> Overall, however, the Zintl phase also shows ionic character due to charge transfer. This mixed nature of bonding, sometimes called Zintl bonding, allows for mediation between ionically and covalently bonded materials.

Despite their curious nature and possible applications in crystalline oxide epitaxy on semiconductors, a relatively modest body of theoretical work exists on Zintl phases (summarized in Refs. 11 and 12). Here, we consider theoretically a Zintl phase SrAl<sub>2</sub> that may find applications in epitaxy of III-V semiconductors with perovskites.<sup>13,14</sup> It crystallizes in the orthorhombic *Imma* structure under ambient conditions and assumes a cubic *Fd-3m* structure under high pressure.<sup>15,16</sup> Here, we focus on the orthorhombic phase. Though hydrogenated SrAl<sub>2</sub>H<sub>2</sub> molecules, where the hydrogen atoms are inserted interstitially, have been recently studied,<sup>11,17</sup> rather little is known about pure SrAl<sub>2</sub> besides the crystallographic data. Therefore, a basic study of its physical properties is of practical interest. We report on the electronic, structural, and elastic properties of bulk SrAl<sub>2</sub> and its low index surfaces. We calculate the work function and surface energy of the (001), (010), and the (100) oriented surfaces of different stoichiometry. For the orthorhombic ground state, we also evaluate the elastic tensor.

**II. COMPUTATIONAL DETAILS**

All calculations are done within the framework of the density functional theory (DFT). We employ the generalized gradient approximation (GGA) with the Perdew-Burke-Ernzerhof functional.<sup>18</sup> To solve the Kohn-Sham equation, we use a plane wave expansion of the wave function along with PAW pseudopotentials as implemented in the VASP code.<sup>19</sup> The valence configuration of Sr is 4s<sup>2</sup>, 4p<sup>6</sup>, 5s<sup>2</sup>, and for Al we use 3s<sup>2</sup>, 3p<sup>1</sup>. The Brillouin zone integration is done using Monkhorst-Pack *k*-point meshes.<sup>20</sup> For primitive cells of orthorhombic and cubic SrAl<sub>2</sub>, we employ 8 × 14 × 8 and 6 × 6 × 6 *k*-point meshes, respectively. Work functions and surface energies are calculated using slab geometry. In these calculations, we use 8 × 14 × 2, 8 × 8 × 2, and 14 × 8 × 2

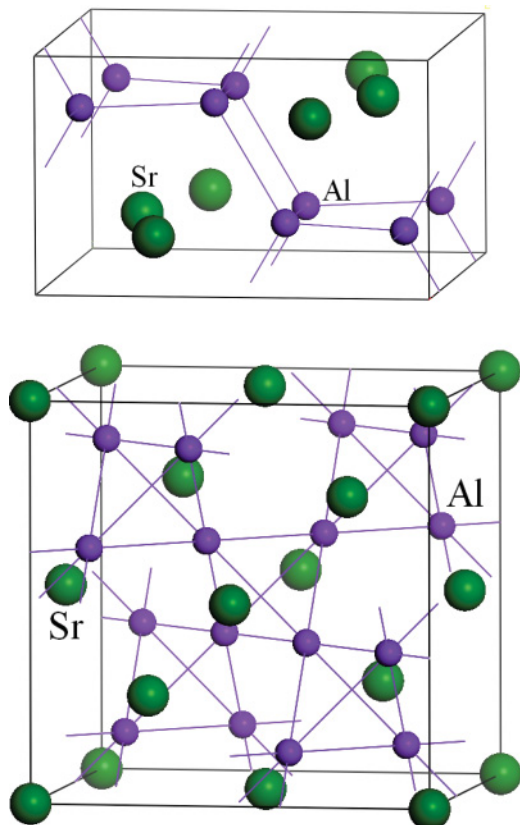


FIG. 1. (Color online) Primitive cells of orthorhombic (a) and cubic (b)  $\text{SrAl}_2$ . The experimental lattice constants are  $7.916 \times 4.813 \times 7.929$  Å for the orthorhombic cell, and 8.291 Å for the cubic cell. The smaller balls are aluminum atoms; the larger balls are strontium atoms.

$k$ -point meshes for the (001), (010), and (100) surface models, respectively. The  $\text{SrAl}_2$  bulk is fully relaxed by optimizing the cell shape, volume, and ionic positions. In the slab calculations, we only allow for ionic relaxation. We use the kinetic energy cutoff of 500 eV. Together with the chosen  $k$ -point meshes, energy convergence is 0.01 meV/cell for bulk calculations. Forces are converged to  $\sim 10$  meV/Å (less than 1 meV/Å in bulk calculations).

### III. BULK PROPERTIES

The primitive cells of orthorhombic and cubic  $\text{SrAl}_2$  are shown in Fig. 1. The orthorhombic cell consists of four molecular  $\text{SrAl}_2$  units, and the cubic cell consists of eight units. The atomic positions in Wyckoff notations are given in Table I. The theoretical lattice constants of the orthorhombic cell are  $a = 7.916$  Å,  $b = 4.813$  Å, and  $c = 7.929$  Å, which are very close to the experimental values of 7.905 Å, 4.801 Å, and 7.974 Å for  $a$ ,  $b$ , and  $c$  respectively.<sup>16</sup> The Al atoms are 4-fold

TABLE I. Atomic positions in Wyckoff notation in orthorhombic and cubic  $\text{SrAl}_2$ .

Orthorhombic	Cubic
4 Sr 4e	8 Sr 8a
8 Al 8i	16 Al 16d

coordinated by other Al atoms with the bond length varying between 2.78 Å and 2.88 Å. Although the Al sublattice does not form a diamond structure, the coordination is consistent with the Zintl-Klemm rules. The theoretical lattice constant of the cubic cell is 8.325 Å (experimental value is 8.291 Å<sup>16</sup>). The cell consists of a diamond Sr sublattice and Al sublattice, which is formed by corner-sharing tetrahedra. In the cubic unit cell, Al atoms are sixfold coordinated by other Al atoms with the Al-Al bond length being 2.93 Å.

The electronic density of states (DOS) normalized per  $\text{SrAl}_2$  molecular unit for both phases is shown in Fig. 2, where the Fermi level is set at zero energy. The semicore Sr 4s and 4p states appear at  $-35$  eV and  $-18$  eV, respectively (not in the figure). The Al 3s states appear between  $-5$  eV and  $-8$  eV in both phases. Close to the Fermi level, the main contributors to the DOS are Al 3p states, Sr 5s states, and  $l = 2$  projected (4d) Sr states. The carrier density within  $\pm k_B T$  around the Fermi level is  $4.9 \times 10^{20} \text{ cm}^{-3}$  in the orthorhombic structure, and it is almost three times higher ( $12.8 \times 10^{20} \text{ cm}^{-3}$ ) in the cubic structure. To put these numbers in perspective, the carrier concentration in commonly used silicide PtSi is  $7.9 \times 10^{20} \text{ cm}^{-3}$ .<sup>21</sup>

We find that the orthorhombic phase is slightly lower (20 meV per unit  $\text{SrAl}_2$ ) in energy than the cubic phase. The experimental work by Cordier *et al.*<sup>16</sup> suggests a pressure-induced phase transition from the orthorhombic to cubic phase at 60 kbar. Theoretically, the transition pressure then can be deduced from

$$E_c + pV_c - TS_c = E_o + pV_o - TS_o. \quad (1)$$

Here  $E$ ,  $V$ , and  $S$  are the internal energy, volume, and entropy, respectively, and  $T$  and  $p$  are temperature and pressure.

The left-hand side is the Gibbs free energy of the cubic phase, and the right-hand side is that of the orthorhombic phase. Ignoring the entropy contribution for the low-temperature limit, the left- and right-hand sides in Eq. (1) are equal at the transition pressure  $p_{\text{trans}}$ , which is the slope of the common tangent of the left- and right-hand side energy in the  $E$ - $V$  diagram. We deduce the volume dependence of the energy in the cubic and orthorhombic phases using constant volume calculations. For a chosen fixed volume value, we fully relax the lattice constants, cell shape, and atomic positions. In Fig. 3, we show the binding energy of the cubic and orthorhombic phases as function of volume per  $\text{SrAl}_2$  unit. The slope of the common tangent is 7.4 kbar, which is somewhat lower than the previously reported theoretical transition pressure of 18 kbar.<sup>22</sup> In Ref. 22, a lower energy cutoff is used, and it is not clear what  $k$ -point density was used for the Brillouin zone integration. In our convergence tests, we find a rather strong dependence of the calculated binding energy on both parameters. We attribute the discrepancy to the differences in the computational setup. Experimentally, the transition pressure is also not entirely clear. Cordier *et al.*<sup>16</sup> performed their experiments at 60 kbar, where the cubic phase was observed. However, the actual phase transition possibly occurs below that pressure. The sample used in this study was most likely polycrystalline, and the temperature is unknown, making a direct comparison difficult. In what follows, we focus only on the orthorhombic structure, as under ambient conditions, it is the lowest-energy phase.

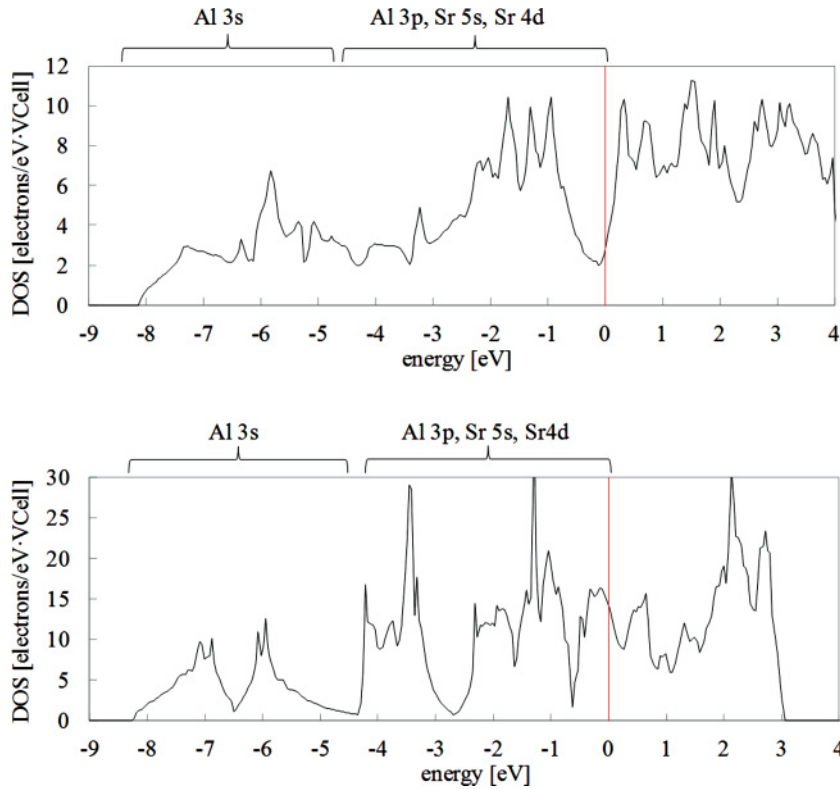


FIG. 2. (Color online) Electronic density of states of orthorhombic (top) and cubic (bottom)  $\text{SrAl}_2$ . The electron carrier density at the Fermi level is three times lower in orthorhombic  $\text{SrAl}_2$  compared to the cubic phase.

#### IV. SURFACE PROPERTIES

We calculate the surface energy of the low-index (001), (010), and (100)  $\text{SrAl}_2$  surfaces using slab geometry. We use  $1 \times 1$  surface cell, and  $\text{SrAl}_2$  slabs are  $\sim 15\text{--}20$  Å thick. Two neighboring slabs are separated by 15 Å vacuum to suppress slab-slab interactions due to the periodic boundary conditions. Our surface models are shown in Fig. 4(a–c). We constructed ten different models (enumerated from one to ten in the figure) according to the following procedure. The dashed lines in Fig. 4 indicate how we cleave each of our ten surfaces. For example, in the (001) orientation, we cut four surfaces: the first one is terminated with Al atoms at the first dashed line, the second surface is terminated with Sr at the second dashed line, and so on. In the (010) orientation, we consider two surfaces:

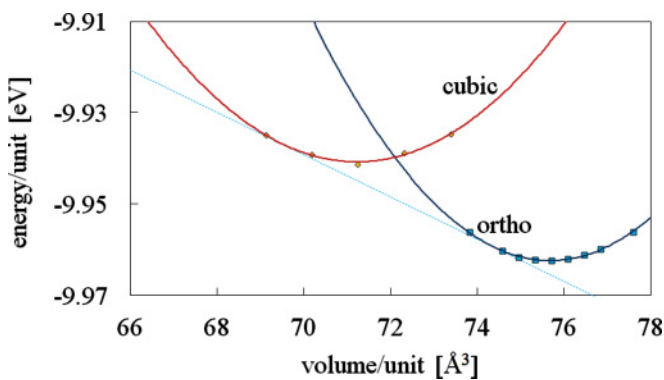


FIG. 3. (Color online) Binding energy of cubic and orthorhombic  $\text{SrAl}_2$  as a function of volume per chemical  $\text{SrAl}_2$  unit. The slope of the common tangent is 7.4 kbar, which is the theoretical transition pressure from the orthorhombic to the cubic phase.

model five as shown in Fig. 4(b) and model six with two top Sr atoms removed. In the (100) orientation, we consider four surfaces. Models seven, eight, and nine are cleaved, as indicated in Fig. 4(c). Model ten is cleaved as in model nine; however, two top Sr atoms are removed. Since most of the surface models are not flat on atomic scale, assigning the surface stoichiometry is somewhat arbitrary. However, when counting all atoms in the slab, our models one, three, five, eight, and ten have the same stoichiometry as bulk  $\text{SrAl}_2$ . However, in models one and eight, Al atoms are facing vacuum, and in models three and ten, Sr atoms are facing vacuum. Only model five has a perfectly stoichiometric surface. Our remaining surfaces are Sr-rich (models two and nine) and Al-rich (models four, six, and seven).

To estimate the surface energy, we use the Gibbs free energy approach:<sup>23</sup>

$$\sigma = [E_{\text{slab}} - N_{\text{Al}}(E_{\text{Al}} + \mu_{\text{Al}}) - N_{\text{Sr}}(E_{\text{Sr}} + \mu_{\text{Sr}})]/2A, \quad (2)$$

where  $E_{\text{slab}}$  is the energy of the slab,  $N_X$  is the number of atomic species X (Al, Sr), and  $\mu_x$  and  $E_x$  are its chemical potential and bulk energy, respectively. The chemical potentials are referenced to bulk energies of metallic Sr and Al. Assuming the equilibrium of the surface with the bulk:

$$\begin{aligned} \mu_{\text{Sr}} + 2\mu_{\text{Al}} &= H_f = -0.788\text{eV}, \\ H_f &< \mu_{\text{Sr}} < 0, \\ H_f &< 2\mu_{\text{Al}} < 0, \end{aligned} \quad (3)$$

we can rewrite Eq. (2) as a function of the chemical potential  $\mu_{\text{Sr}}$  solely:

$$\begin{aligned} \sigma &= [E_{\text{slab}} - N_{\text{Sr}}E_{\text{Sr}} - N_{\text{Al}}(E_{\text{Al}} + 0.5H_f) \\ &\quad - \mu_{\text{Sr}}(N_{\text{Sr}} - 0.5N_{\text{Al}})]/2A, H_f < \mu_{\text{Sr}} < 0. \end{aligned} \quad (4)$$

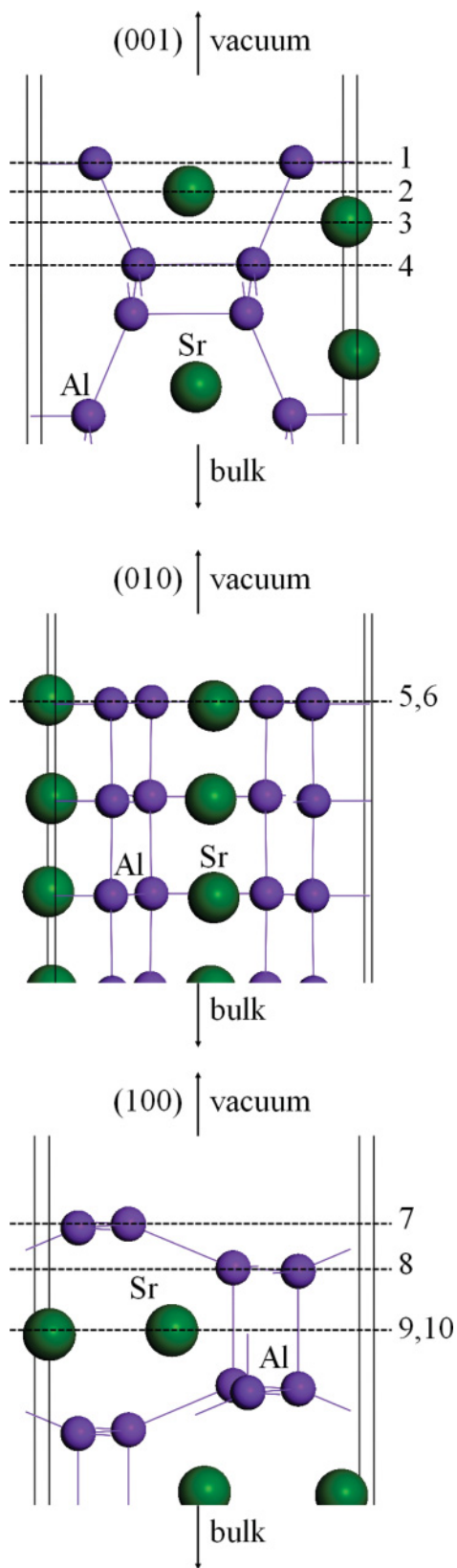


FIG. 4. (Color online) Surface models with (a) (001) orientation, (b) (010) orientation and (c) (100) orientation. From the three models shown, we deduce ten surface models in total. The dashed lines indicate how we cleave our surfaces. In total, we have four (001) oriented surface models, two (010) oriented surface models, and four (100) oriented surface models.

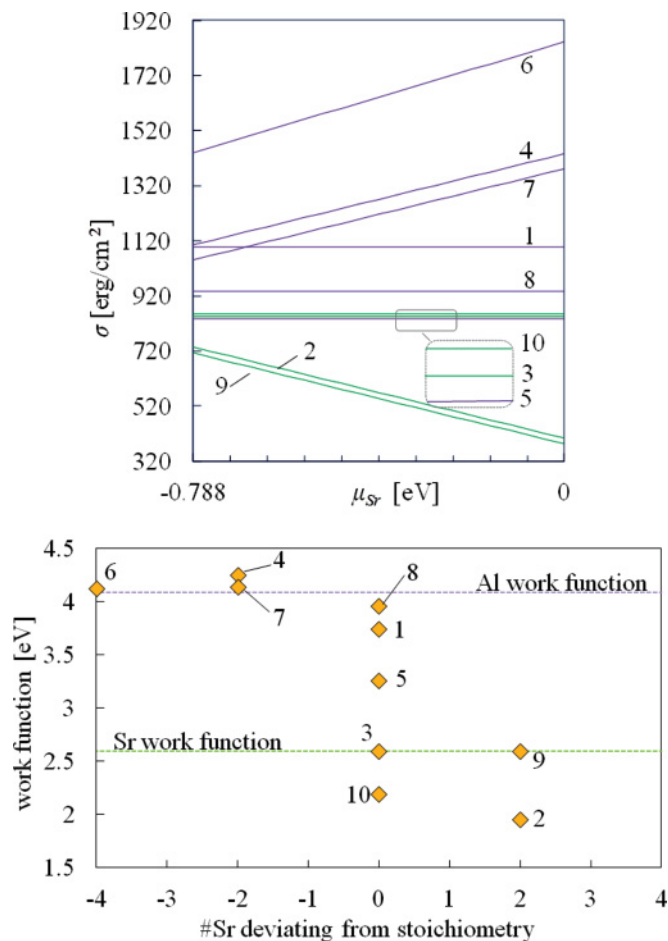


FIG. 5. (Color online) (a) Surface energy of orthorhombic  $\text{SrAl}_2$  as a function of the chemical potential of Sr. The data labels indicate our model numbers. Sr-terminated surfaces tend to have lower surface energy than the stoichiometric or Al-terminated surfaces. The running numbers indicate the model. (b) Work function of orthorhombic  $\text{SrAl}_2$ . The x axis shows the deviation of the slab from the  $\text{SrAl}_2$  stoichiometry. The data labels indicate the model number. The work function is strongly termination dependent.

The boundary conditions for  $\mu_{\text{Sr}}$  correspond to Sr-poor experimental conditions for  $\mu_{\text{Sr}} = H_f$  and Sr-rich conditions for  $\mu_{\text{Sr}} = 0$ . We show the surface energy in Fig. 5(a). Our surface models are indicated in the plot. The surface energy ranges between 320 erg/cm<sup>2</sup> and 1842 erg/cm<sup>2</sup>, depending on the chemical environment. Over the entire range of the chemical potential, the (100) oriented Sr-rich surface model nine has the lowest energy, and it is closely followed by the (001) oriented surface model two of the same stoichiometry. Al-terminated surfaces (models four, six and seven) have approximately 300 erg/cm<sup>2</sup> higher surface energy under Sr-poor conditions, and approximately 900 erg/cm<sup>2</sup> higher surface energy under Sr-rich conditions. The remaining five surfaces have surface energy ranging between 950 erg/cm<sup>2</sup> and 1100 erg/cm<sup>2</sup>. This is important when considering the wetting behavior of thin  $\text{SrAl}_2$  films on a substrate. A possible substrate is STO. Its lattice mismatch to  $\text{SrAl}_2$  is less than 0.5% for some configurations. The surface energy of STO

ranges from 801 erg/cm<sup>2</sup> to 1923 erg/cm<sup>2</sup>, depending on the chemical environment.<sup>24</sup> Thus, SrAl<sub>2</sub> could wet STO for two Sr-rich models with the lowest surface energy. A more detailed study including the interface is necessary to address this question, however, and is under way.

For all SrAl<sub>2</sub> surfaces considered here, we calculate the work function. The thickness of our SrAl<sub>2</sub> slabs is approximately 20 Å, which is sufficient to mimic the bulk electronic properties deep inside the slab. We calculate the electrostatic potential in the simulation cell and average it over the *xy* plane for each *z* value, where *z* runs in the direction normal to the surface. We then averaged the microscopic *V(z)* along the *z* axis over the bulk and vacuum regions. The energy difference between the value of the averaged potential in the vacuum region and the Fermi level of the slab is taken to be the work function. The calculated values of the work function are shown in Fig. 5(b). The labels indicate the model number. We included the work functions of Sr and Al metals for comparison. The *x* axis indicates the number of strontium atoms by which a given slab deviates from the bulk 1:2 stoichiometry. Negative values indicate Al-rich slabs, and positive values correspond to Sr-rich slabs. The work function for Al-rich slabs is close to 4.08 eV of Al metal, whereas for Sr-rich models, it ranges from 2.6 eV (work function of pure Sr metal) to 2.0 eV. The lowest-surface-energy models have work functions of 2.0 eV [model two in Fig. 4(b), (001) orientation] and 2.6 eV [model nine in Fig. 4(b), (100) orientation]. For the stoichiometric conditions, i.e., twice as many Al atoms as Sr atoms in the slab, the work function ranges from 2.2 eV (model ten) to 4.0 eV (model eight). Surface models one and eight have Al atoms closest to vacuum, resulting in the highest work function among the stoichiometric models. Models three and ten have Sr atoms closest to vacuum, giving the lowest work function among the stoichiometric models. Interestingly, our model five has Sr and Al atoms equally close to the vacuum region. This model has a work function of 3.25 eV, which is roughly the average of work functions of Sr and Al. The main conclusion we draw from Fig. 5(b) is that the work function depends mainly on the surface chemistry. For the models with Al at the surface, the work function tends to be close to that of Al metal, whereas the work function of surfaces with mainly Sr on top is close to the work function of Sr metal.

## V. ELASTIC PROPERTIES

Because strain plays an important role in epitaxy, we calculate the elastic constants of orthorhombic SrAl<sub>2</sub> from first principles. Generally, the energy of a strained system can be written as a second-order expansion in the distortion parameters  $\alpha_{i,j}$ :<sup>25</sup>

$$E(V, \alpha) = E(V_0, 0) + \frac{V_0}{2} \sum_{a,b,c,d} C_{abcd} \alpha_{ab} \alpha_{cd}. \quad (5)$$

The first-order term drops out as the expansion is about the ground state (*V*<sub>0</sub> is the ground state volume of the cell). The second-order term is described by the adiabatic elastic constants *C<sub>abcd</sub>*. However, *C<sub>abcd</sub>* and  $\alpha_{ab}$  are not all independent, and using Voigt notation, Eq. (5) can be

TABLE II. Elastic constants and bulk modulus of orthorhombic SrAl<sub>2</sub>. The elastic constants meet the Cauchy mechanical stability requirements.<sup>26</sup> The bulk modulus is close to that of Al metal (7.6 dyn/cm<sup>2</sup>).

	Elastic constant (10 <sup>11</sup> dyn/cm <sup>2</sup> )
<i>C</i> <sub>11</sub>	8.55
<i>C</i> <sub>12</sub>	8.76
<i>C</i> <sub>13</sub>	7.68
<i>C</i> <sub>22</sub>	9.01
<i>C</i> <sub>23</sub>	7.91
<i>C</i> <sub>33</sub>	6.84
<i>C</i> <sub>44</sub>	4.28
<i>C</i> <sub>55</sub>	3.51
<i>C</i> <sub>66</sub>	3.50
<i>B</i>	8.12

simplified. There are nine independent elastic constants in an orthorhombic crystal: *C*<sub>11</sub>, *C*<sub>12</sub>, *C*<sub>13</sub>, *C*<sub>22</sub>, *C*<sub>23</sub>, *C*<sub>33</sub>, *C*<sub>44</sub>, *C*<sub>55</sub>, and *C*<sub>66</sub>. In order to determine these constants, nine independent distortions must be applied to the system. We use the distortions suggested in Ref. 25. Equation (5) is valid for small distortions, and to have a measure of “small,” we compare the volume changes after applying a specific distortion. Our distortion parameters are within the range ±0.02, with a maximum volume change of ±6 Å<sup>3</sup> or 2% of *V*<sub>0</sub>. We relax the atomic positions for all distortions. Using a quadratic fit to the calculated binding energy, we extract the elastic constants *C<sub>ij</sub>*. The results are summarized in Table II. The elastic constants meet the Cauchy mechanical stability requirements.<sup>26</sup> The bulk modulus is given by

$$B = \frac{1}{9}(C_{11} + C_{22} + C_{33} + 2C_{12} + 2C_{13} + 2C_{23}) \\ = 8.12 \times 10^{11} \text{ dyn/cm}^2. \quad (6)$$

Interestingly, the bulk modulus of SrAl<sub>2</sub> is comparable to aluminum’s 7.6 × 10<sup>11</sup> dyn/cm<sup>2</sup>. The bulk modulus of Sr is only 1.2 × 10<sup>11</sup> dyn/cm<sup>2</sup>. Unfortunately, no data on the elastic properties of SrAl<sub>2</sub> are available in the literature, making a comparison impossible.

## VI. CONCLUSIONS

In summary, we have theoretically investigated the electronic structure and elastic and surface properties of cubic and orthorhombic SrAl<sub>2</sub> using density functional theory. We predict a significant increase in the electric conductivity of the cubic phase compared to the ground state orthorhombic phase. We estimate the transition pressure of the orthorhombic to cubic transformation to be significantly lower than that reported in a recent experimental study. The elastic constants of orthorhombic SrAl<sub>2</sub> are reported; the bulk modulus of 8.12 × 10<sup>11</sup> dyn/cm<sup>2</sup> makes SrAl<sub>2</sub> slightly stiffer than Al metal. The work function and surface energy depend strongly on the surface termination. The Sr-terminated surface has lower surface energy and work function close to 2.59 eV of Sr metal,

while the Al-terminated surface has a higher surface energy and work function close to 4.08 eV of Al metal. The work function result is consistent with the transistor data reported in Ref. 27, where the Al surface of a SrAl Zintl interlayer was used to achieve wetting of SrTiO<sub>3</sub> by GaAs.

### ACKNOWLEDGMENTS

This work is supported by the National Science Foundation under Grant No. DMR1006725, and Texas Advanced Computing Center.

\*demkov@physics.utexas.edu

- <sup>1</sup>D. A. Muller, *Nature* **399**, 758 (1999).
- <sup>2</sup>T. N. Theis and P.M. Solomon, *Science* **327**, 1600 (2010).
- <sup>3</sup>A. A. Demkov and A. Navrotsky, Eds., *Materials Fundamentals of Gate Dielectrics* (Springer, Dordrecht, 2005).
- <sup>4</sup>R. Droopad, K. Eisenbeiser, and A. A. Demkov, in *High Dielectric Constant Materials*, edited by H. Huff and D. Gilmer (Springer, Berlin, 2004), pp. 639-666.
- <sup>5</sup>J. Robertson, *Eur. Phys. J. Appl. Phys.* **28**, 265 (2004).
- <sup>6</sup>R. A. McKee, F. J. Walker, and M. F. Chisholm, *Phys. Rev. Lett.* **81**, 3014 (1998).
- <sup>7</sup>X. Zhang, A. A. Demkov, H. Li, X. Hu, Y. Wei, and J. Kulik, *Phys. Rev. B* **68**, 125323 (2003).
- <sup>8</sup>R. A. McKee, F. J. Walker, and M. F. Chisholm, *Phys. Rev. Lett.* **81**, 3014 (1998).
- <sup>9</sup>A. A. Demkov and X. Zhang, *J. Appl. Phys.* **103**, 103710 (2008).
- <sup>10</sup>E. Zintl and W. Dullenkopf, *Z. Phys. Chem. B* **16**, 195 (1932).
- <sup>11</sup>Thomas Fässler, *Zintl Phases: Principles and Recent Developments*, Vol. 139 (Springer, Berlin, Heidelberg, New York, 2011).
- <sup>12</sup>S. M. Kauzlarich, *Chemistry, Structure, and Bonding of Zintl Phases and Ions* (VCH Publishers, Inc., New York, 1996).
- <sup>13</sup>Y. Liang and A. A. Demkov, in *Materials Fundamentals of Gate Dielectrics*, edited by A. A. Demkov and A. Navrotsky (Springer, Berlin, 2005), pp. 313-348.
- <sup>14</sup>A. A. Demkov, H. Seo, X. Zhang, and J. Ramdani, *Appl. Phys. Lett.* **100**, 071602 (2012).
- <sup>15</sup>G. Nagorsen, H. Posch, H. Schaefer, and A. Weiss, *Z. Naturforsch. B* **24**, 1191 (1969).
- <sup>16</sup>G. Cordier, E. Czech, and H. Schaefer, *Z. Naturforsch. B* **37**, 1442 (1982).
- <sup>17</sup>F. Gingl, T. Vogt, and E. Akiba, *J. Alloys Compd.* **306**, 127 (2000).
- <sup>18</sup>J. P. Perdew, K. Burke, and M. Ernzerhof, *Phys. Rev. Lett.* **77**, 3865 (1996).
- <sup>19</sup>G. Kresse and J. Hafner, *Phys. Rev. B* **47**, 558 (1993); G. Kresse and J. Furthmüller, *Comput. Mat. Sci.* **6**, 15 (1996); *Phys. Rev. B* **54**, 11169 (1996); G. Kresse and J. Hafner, *J. Phys: Condens. Matt.* **6**, 8245 (1994); G. Kresse and D. Joubert, *Phys. Rev. B* **59**, 1758 (1999).
- <sup>20</sup>H. J. Monkhorst and J. D. Pack, *Phys. Rev. B* **13**, 5188 (1976).
- <sup>21</sup>A. Slepko and A. A. Demkov, *Phys. Rev. B* **85**, 035311 (2012).
- <sup>22</sup>S. Kal, E. Stoyanov, J.-P. Belieres, T. L. Groy, R. Norrestam, and U. Häussermann, *J. Sol. State Chem.* **181**, 3016 (2008).
- <sup>23</sup>G.-X. Qian, R. M. Martin, and D. J. Chadi, *Phys. Rev. B* **38**, 7649 (1988).
- <sup>24</sup>A. A. Demkov, *Phys. Status Solidi B* **226**, 57 (2001).
- <sup>25</sup>D. C. Wallace, *Solid State Physics* **25**, 302 (1970).
- <sup>26</sup>O. Beckstein, J. E. Klepeis, G. L. W. Hart, and O. Pankratov, *Phys. Rev. B* **63**, 134112 (2001).
- <sup>27</sup>K. Eisenbeiser, R. Emrick, R. Droopad, Z. Yu, J. Finder, S. Rockwell, J. Holmes, C. Overgaard, and W. Ooms, *IEEE Electron Device Lett.* **23**, 300 (2002).